

Anti-apoptotic gene *Bcl2* is required for stapes development and hearing

MR Carpinelli^{1,2,3}, AK Wise⁴, BD Arhatari⁵, P Bouillet^{2,6}, SSM Manji^{3,7}, MG Manning^{1,3}, AA Cooray^{2,3} and RA Burt^{1,2,3,8}

In this paper we describe novel and specific roles for the apoptotic regulators Bcl2 and Bim in hearing and stapes development. Bcl2 is anti-apoptotic while Bim is pro-apoptotic. Characterization of the auditory systems of mice deficient for these molecules revealed that *Bcl2*^{-/-} mice suffered severe hearing loss. This was conductive in nature and did not affect sensory cells of the inner ear, with cochlear hair cells and neurons present and functional. *Bcl2*^{-/-} mice were found to have a malformed, often monocrucral, porous stapes (the small stirrup-shaped bone of the middle ear), but a normally shaped malleus and incus. The deformed stapes was discontinuous with the incus and sometimes fused to the temporal bones. The defect was completely rescued in *Bcl2*^{-/-} *Bim*^{-/-} mice and partially rescued in *Bcl2*^{-/-} *Bim*^{+/-} mice, which displayed high-frequency hearing loss and thickening of the stapes anterior crus. The *Bcl2*^{-/-} defect arose *in utero* before or during the cartilage stage of stapes development. These results implicate Bcl2 and Bim in regulating survival of second pharyngeal arch or neural crest cells that give rise to the stapes during embryonic development.

Cell Death and Disease (2012) 3, e362; doi:10.1038/cddis.2012.100; published online 9 August 2012

Subject Category: Neuroscience

Apoptosis is required for developmental morphogenesis¹ and disruption of this pathway can lead to developmental defects. Regulation of apoptosis is conferred by families of pro- and anti-apoptotic molecules, combinations of which are active in specific cell types and stages of development. The anti-apoptotic protein Bcl2 acts by binding and antagonising executioner molecules Bax and Bak. In response to apoptotic stimuli, such as growth factor deprivation or ultraviolet radiation, the pro-apoptotic protein Bim binds to and antagonises Bcl2. This releases Bax and Bak, allowing them to permeabilise the mitochondrial outer membrane. The resultant release of cytochrome *c* leads to activation of caspases, enzymes that dismantle the cell.² Bcl2 and Bim are partially functionally redundant with other anti- and pro-apoptotic protein family members respectively.² Despite this, deficiencies of Bcl2 or Bim cause widespread problems. *Bcl2*^{-/-} mice display runting, small ear pinnae, craniofacial abnormalities, premature greying, lymphopenia, polycystic kidney disease and premature death.³ On a mixed 129 Sv/C57BL/6 genetic background, *Bim*^{-/-} mice display leukocytosis and autoimmune kidney disease, which is lethal at 1 year of age.⁴ The *Bcl2*^{-/-} phenotype is rescued in *Bcl2*^{-/-} *Bim*^{-/-} mice and partially rescued in *Bcl2*^{-/-} *Bim*^{+/-} mice.⁵ Removal of

both Bcl2 and Bim is believed to restore the balance between pro- and anti-apoptotic protein levels, leading to appropriate levels of developmental and homeostatic apoptosis. Despite observations of the deformed *Bcl2*^{-/-} mouse pinna,³ and Bcl2 expression in the mesenchymal cells from which the pinna develops,⁶ no characterisation of the animals' hearing had been conducted. We tested the hearing of these mice in order to determine whether Bcl2 is required for survival of sensory hair cells in the cochlea. These cells convert sound into signals that travel along the auditory nerve to the brain. Both hair cells and auditory neurons are essential for hearing.⁷ We found that, although cochlear hair cells are present, *Bcl2*^{-/-} mice have severe hearing loss due to a developmental stapes defect.

Results

The hearing of wild-type, *Bcl2*^{-/-}, *Bim*^{-/-}, *Bcl2*^{-/-} *Bim*^{+/-} and *Bcl2*^{-/-} *Bim*^{-/-} mice was assessed using auditory brainstem response (ABR)-testing. ABR thresholds of *Bcl2*^{-/-} mice were increased by >60 dB sound pressure level (SPL) at 16 kHz compared with wild-type littermates (Figure 1a). *Bcl2*^{-/-} *Bim*^{-/-} mice displayed normal ABR

¹Molecular Hearing Laboratory, The Murdoch Children's Research Institute, Royal Children's Hospital, 50 Flemington Road, Parkville, Victoria 3052, Australia; ²The Walter and Eliza Hall Institute of Medical Research, 4 Research Avenue, La Trobe Research and Development Park, Bundoora, Victoria 3086, Australia; ³The Hearing Cooperative Research Centre, 550 Swanston Street, Melbourne, Victoria 3010, Australia; ⁴Bionics Institute, 384-388 Albert Street, East Melbourne, Victoria 3002, Australia; ⁵Department of Physics, La Trobe University, Victoria 3086, Australia; ⁶Department of Medical Biology, University of Melbourne, Melbourne, Victoria 3010, Australia; ⁷Department of Otolaryngology, The University of Melbourne, 32 Gisborne Street, East Melbourne, Victoria 3002, Australia and ⁸Department of Genetics, University of Melbourne, Victoria 3010, Australia

*Corresponding author: MR Carpinelli, Molecular Hearing Laboratory, The Murdoch Children's Research Institute, Royal Children's Hospital, 50 Flemington Road, Parkville, Victoria 3052, Australia. Tel: +61 3 993 66797; Fax: +61 3 934 81391; E-mail: marina.carpinelli@mcri.edu.au

Keywords: Bcl2; Bim; stapes; conductive hearing loss; monocrucral; second pharyngeal arch

Abbreviations: +ve, positive; 3D, three-dimensional; -ve, negative; ABR, auditory brainstem response; bp, base pairs; CCD, charge-coupled device; dB, decibel; e8, embryonic day eight; eABR, electrically-evoked auditory brainstem response; kHz, kilohertz; NBF, neutral-buffered formalin; p21, postnatal day twenty-one; PBS, phosphate-buffered saline; PCR, polymerase chain reaction; p.e., peak equivalent; SEM, standard error of the mean; SGN, spiral ganglion neuron; SPL, sound pressure level; X μ CT, x-ray micro-computed tomography

Received 13.12.11; revised 21.6.12; accepted 22.6.12; Edited by A Verkhatsky

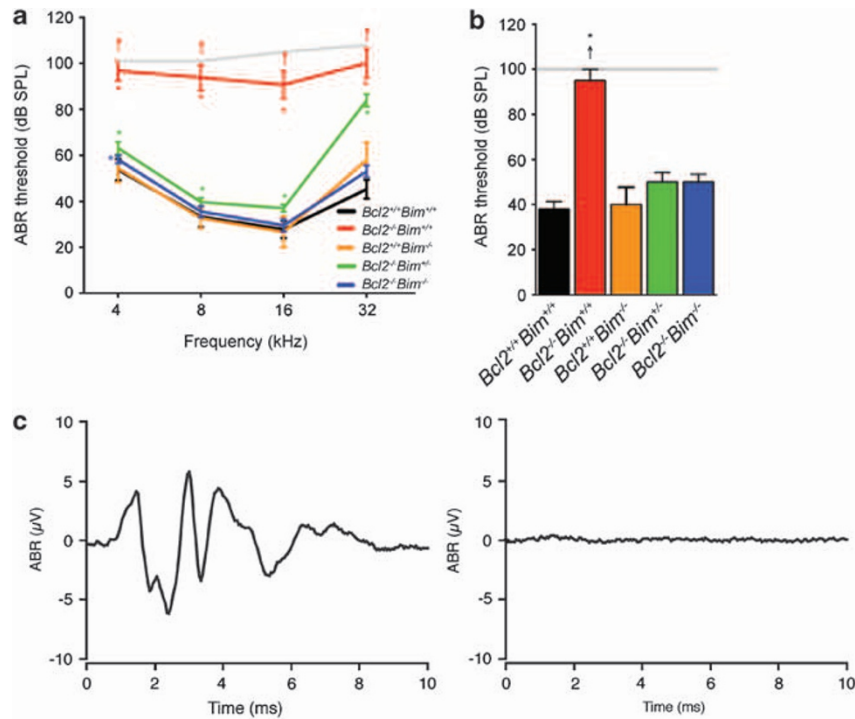


Figure 1 Mean ABR thresholds to (a) tone-pip and (b) click stimuli at 3–8 weeks of age; $Bcl2^{+/+} Bim^{+/+}$ $n=10$; $Bcl2^{-/-} Bim^{+/+}$ $n=7$; $Bcl2^{+/+} Bim^{-/-}$ $n=3$; $Bcl2^{-/-} Bim^{+/+}$ $n=6$; $Bcl2^{-/-} Bim^{-/-}$ $n=6$; arrows indicate when some mice of that genotype had no ABR to the loudest sound presented (grey line); (c) representative ABR trace to 100 dB SPL click in $Bcl2^{+/+}$ and (d) $Bcl2^{-/-}$ mouse; * $P<0.05$; Error bars = S.E.M.

thresholds and $Bcl2^{-/-} Bim^{+/+}$ mice exhibited high-frequency hearing loss. $Bcl2^{-/-}$ mice displayed a similar ABR threshold shift to click (mixed frequency) stimuli (Figure 1b). The severity of the $Bcl2^{-/-}$ hearing loss was illustrated by comparing the ABR trace elicited by a 100 dB SPL click for a wild-type mouse (Figure 1c) and a $Bcl2^{-/-}$ mouse (Figure 1d). These results indicated that $Bcl2^{-/-}$ mice were profoundly deaf at 3 weeks of age, soon after auditory development is complete.

Bcl2 is widely expressed in neurons in human fetuses and adults and is also expressed in foetal cochlear hair cells.^{6,8} We hypothesised that the hearing loss in $Bcl2^{-/-}$ mice may be due to premature apoptosis of cochlear hair cells or neurons. We tested this hypothesis by examining mid-modiolar sections of the cochlea stained with hematoxylin and eosin. Low-power photomicrographs (Figures 2a, d, g and j) revealed that the gross cochlear structure was normal in $Bcl2^{+/+} Bim^{+/+}$, $Bcl2^{-/-} Bim^{+/+}$, $Bcl2^{-/-} Bim^{+/+}$ and $Bcl2^{-/-} Bim^{-/-}$ mice. High-power photomicrographs of organ of Corti (Figures 2b, e, h and k) revealed a single row of inner hair cells and three rows of outer hair cells to be present in all mice. High-power photomicrographs of Rosenthal's canal (Figures 2c, f, i and l) indicated that spiral ganglion neurons (SGNs) were present in all mice. We found no difference in the density of these neurons between wild-type, $Bcl2^{-/-}$, $Bcl2^{-/-} Bim^{+/+}$ or $Bcl2^{-/-} Bim^{-/-}$ mice (Supplementary Figure 1). These results indicated that *Bcl2* is not required for survival of cochlear hair cells or SGN during development.

To assess the functional capacity of the inner ear, $Bcl2^{-/-}$ mice were subjected to an electrically-evoked auditory

brainstem response (eABR) test.⁹ $Bcl2^{-/-}$ mice generated evoked responses to electrical stimulation, indicating that the inner ear and auditory neural circuitry was functional. There was no difference in eABR thresholds between $Bcl2^{+/+}$ and $Bcl2^{-/-}$ mice (Supplementary Figure 2). These results suggest that $Bcl2^{-/-}$ hearing loss is not due to an inability of the SGN or higher auditory centres to initiate and conduct action potentials.

The malleus, incus and stapes are middle ear bones (ossicles) that mechanically conduct sound from the tympanic membrane to the cochlea.¹⁰ Defects in the ossicular chain cause conductive hearing loss. X-ray micro-computed tomography ($X_{\mu}CT$) scanning of ears revealed defects in the $Bcl2^{-/-}$ ossicular chain. The stapes was malformed in all $Bcl2^{-/-}$ animals examined. Normally the stapes is stirrup-shaped with a head contacting the incus and a footplate embedded into the oval window membrane.¹⁰ The stapedia artery runs through the hole in the stirrup, or obturator foramen, and the stapedia muscle attaches to a protrusion on the posterior crus called the tubercle.¹⁰ Scans of wild-type (Figure 3a) and $Bcl2^{-/-}$ (Figure 3b) middle ears revealed that the $Bcl2^{-/-}$ stapes was inserted into the oval window of the cochlea but that the crura were deformed. Scans of wild-type (Figure 3c) and $Bcl2^{-/-}$ (Figure 3d) left ears revealed the absence of a posterior crus and discontinuity between the stapes and incus in $Bcl2^{-/-}$ mice. Scans of wild-type (Figure 3e) and $Bcl2^{-/-}$ (Figures 3f, g and h) right ears revealed that the $Bcl2^{-/-}$ stapes was sometimes fused to the styloid process at the tubercle via a bone bridge and sometimes displayed thinning of the posterior crus and thickening of the anterior crus.

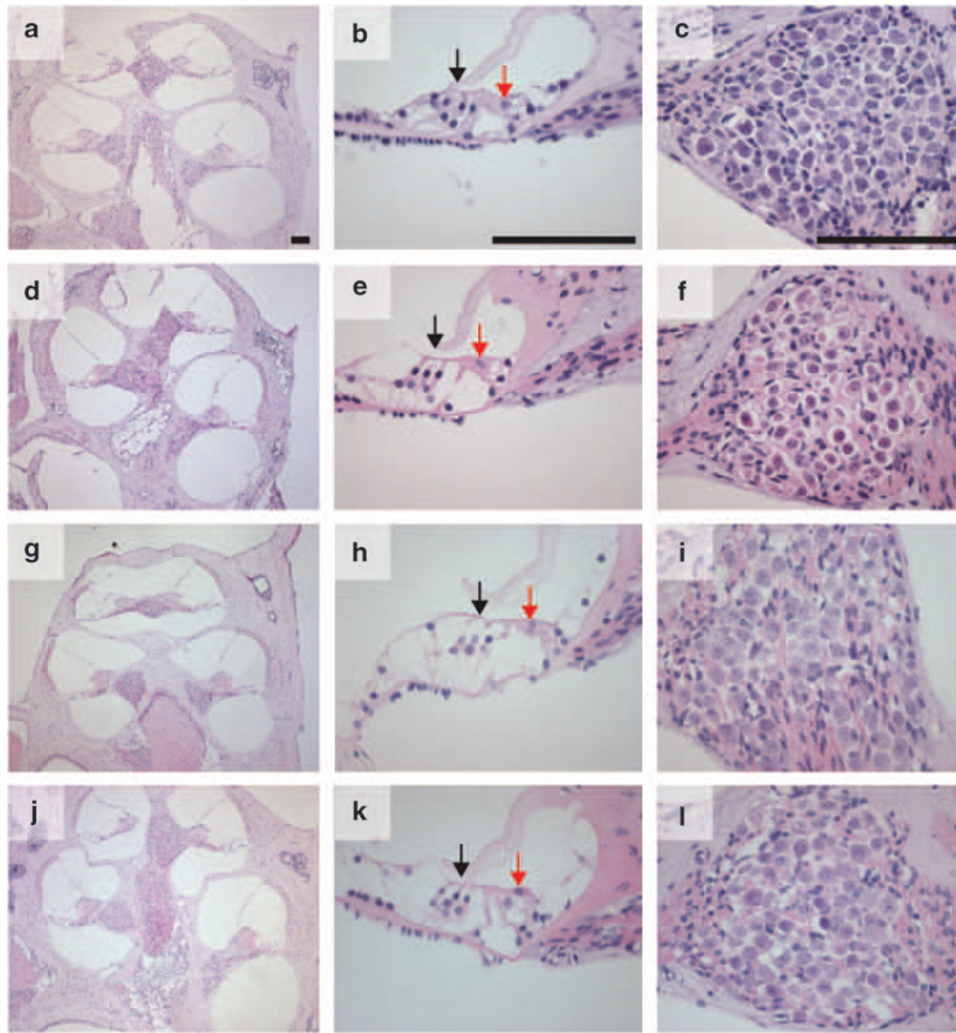


Figure 2 Light micrographs of mid-modiolar cochlea sections stained with hematoxylin and eosin; left panel shows cochlea at low magnification; middle panel shows middle turn organ of Corti with inner and outer hair cells indicated by red and black arrows respectively; right panel shows middle turn Rosenthal's canal, which contains SGN; (a–c) *Bcl2*^{+/+} *Bim*^{+/+}; (d–f) *Bcl2*^{-/-} *Bim*^{+/+}; (g–i) *Bcl2*^{-/-} *Bim*^{+/-}; (j–l) *Bcl2*^{-/-} *Bim*^{-/-}; bar 100 μ m. No histological difference is discernible between mice, all of which were 3–8 weeks of age

Light microscopic examination of wild-type (Figure 4a) and *Bcl2*^{-/-} (Figure 4b) stapes showed the absence of the posterior crus and thickening of the anterior crus in *Bcl2*^{-/-} mice. The *Bcl2*^{-/-} *Bim*^{+/-} stapes (Figure 4c) had slight thickening of the anterior crus and the *Bcl2*^{-/-} *Bim*^{-/-} stapes (Figure 4d) was normal.

The *Bcl2*^{-/-} stapes were abnormally soft and fragile during dissection. This suggested that the internal structure of this ossicle was abnormal. We collected histological sections of ossicles and stained them with hematoxylin and eosin. Photomicrographs showed that the wild-type stapes (Figure 5a) was composed of solid bone while the *Bcl2*^{-/-} stapes (Figure 5b) was porous, containing erythrocytes and other cells not usually present. Neither of the *Bcl2*^{-/-} *Bim*^{-/-} (Figure 5c) or *Bcl2*^{-/-} *Bim*^{+/-} (Figure 5d) stapes displayed the porous phenotype. The wild-type (Figure 5e) and *Bcl2*^{-/-} (Figure 5f) malleus and wild-type (Figure 5g) and *Bcl2*^{-/-} (Figure 5h) incus also did not show the porous phenotype.

Postnatal development of the *Bcl2*^{-/-} stapes was examined using skeletal preparations of the mouse skull stained with alcian blue and alizarin red. Cartilage appeared blue and bone appeared pink in these preparations. At birth, mouse ossicles are cartilaginous.¹¹ They undergo endochondral ossification, in which cartilage is replaced by bone,¹⁰ and bone remodelling, in which bone is resorbed by osteoclasts and laid down by osteoblasts, to attain their mature shape by postnatal day 21 (p21). The wild-type stapes was annular at p0 (Figure 6a) while the *Bcl2*^{-/-} stapes was monocrucial (Figure 6g). Alcian blue staining indicated that the stapes was made of cartilage at this stage. The stapes remained cartilaginous at p1 (Figures 6b and h) and p4 (Figures 6c and i). By p7 (Figures 6d and j) the stapes had ossified and grown in size. By p13 (Figures 6e and k) the stapes had undergone bone remodelling to change shape and further remodelling allowed the stapes to attain its mature shape by p21 (Figures 6f and l). The *Bcl2*^{-/-} stapes underwent

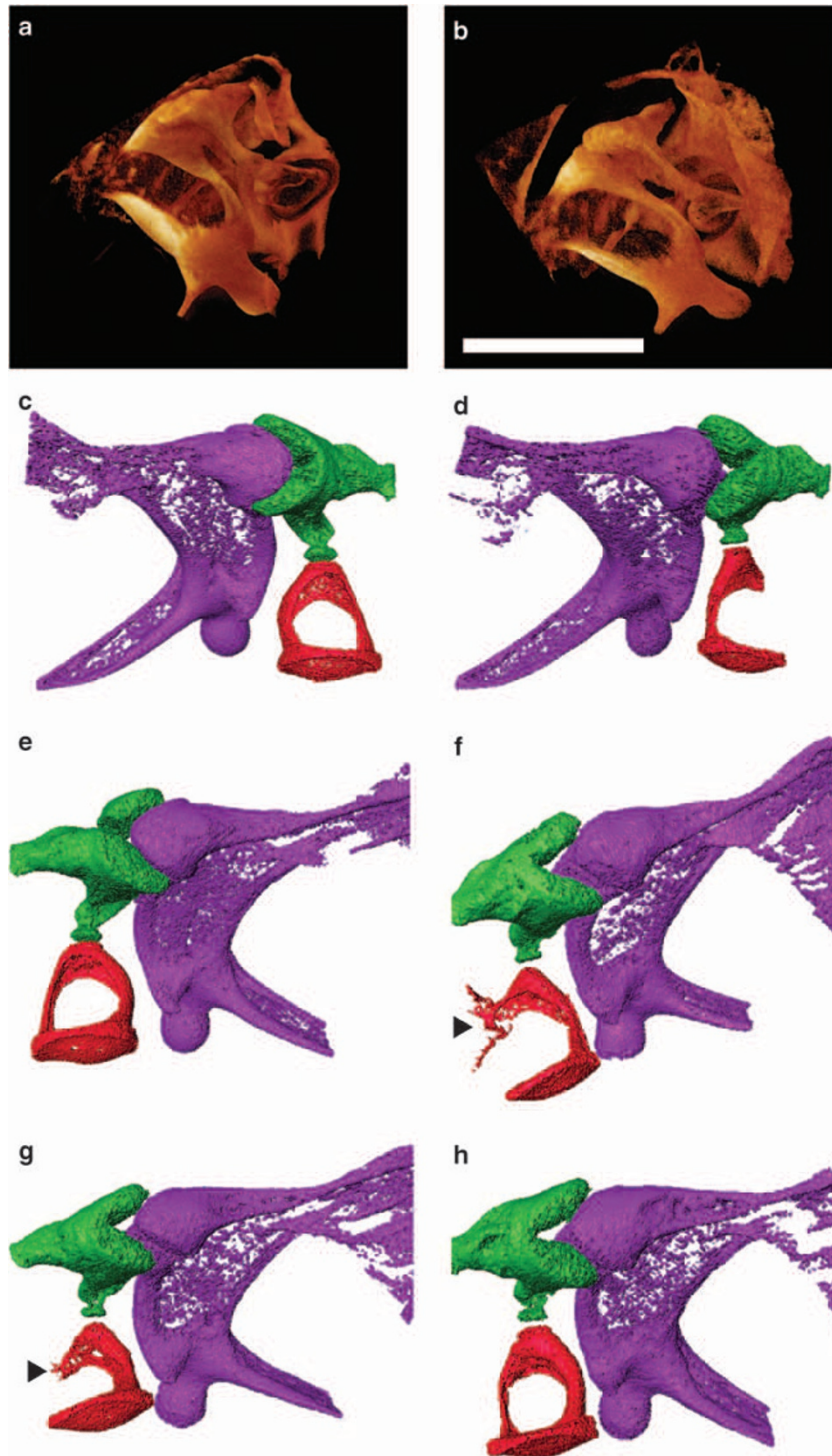


Figure 3 X μ CT images of middle ear showing the various *Bcl2*^{-/-} stapes malformations. Both (a) *Bcl2*^{+/+} and (b) *Bcl2*^{-/-} left ear stapes have footplates inserted into the cochlear oval window. Images in (c–h) show ossicles with the malleus colored purple, incus green and stapes red. (c) *Bcl2*^{+/+} and (d) *Bcl2*^{-/-} left ear ossicles showing the absence of posterior crus in the knockout mice. (e) *Bcl2*^{+/+} and (f–h) *Bcl2*^{-/-} right ear ossicles showing two stapes with fusions to styloid process at tubercle (arrowheads) and one bicrucial stapes with thin posterior crus and thick anterior crus; all mice were 3 weeks of age; bar 0.5 mm

ossification at the same time as the wild-type stapes and underwent bone remodelling between p7 and p21. These results showed that the malformation of the *Bcl2*^{-/-} stapes arose *in utero* and was not caused by defects in ossification or bone remodelling.

Discussion

The aim of this study was to determine whether the apoptotic regulators Bcl2 and Bim regulate sensory hair cell survival in the inner ear. Our characterisation of the auditory system of

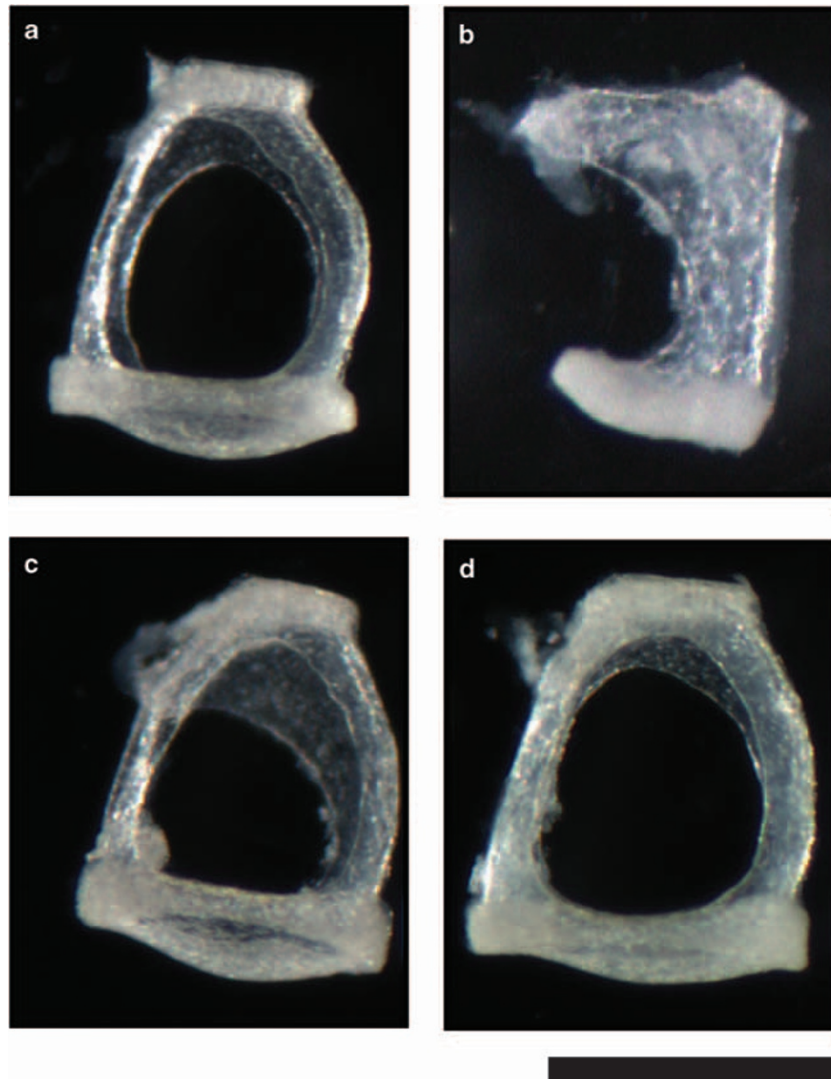


Figure 4 Light micrographs showing monocrucral *Bcl2*^{-/-} stapes composed of abnormal bone and *Bcl2*^{-/-}*Bim*^{+/-} stapes with thickening of anterior crus. (a) *Bcl2*^{+/+} *Bim*^{+/+}; (b) *Bcl2*^{-/-} *Bim*^{+/+}; (c) *Bcl2*^{-/-} *Bim*^{+/-}; (d) *Bcl2*^{-/-} *Bim*^{-/-}; all mice were 3–8 weeks of age; bar 0.5 mm

mice lacking these proteins reveals that Bcl2/Bim interplay is not required for development or function of the cells of the inner ear. This is despite the expression of Bcl2 in cochlear hair cells and widespread expression in neurons. Bcl2 may have a redundant role or no role at all in the survival of these cells. However, *Bcl2*^{-/-} mice display severe hearing loss due to impaired development of the stapes in the middle ear. This is likely due to increased apoptosis in the neural crest or second pharyngeal arch cells that give rise to the stapes.

On day 8 of mouse embryonic development (e8), cells migrate from the neural crest to the first and second pharyngeal arches.¹⁰ Cells forming the malleus and incus migrate from the first and second rhombomeres and caudal mesencephalon in the neural crest to the first pharyngeal arch.¹⁰ Cells forming the stapes migrate mainly from the fourth rhombomere to the second pharyngeal arch, with small contributions from rhombomeres three and five.^{10,12} This arch also gives rise to most of the pinna,¹⁰ which is abnormally

small in *Bcl2*^{-/-} mice. Furthermore, *Bcl2* is expressed in the condensation of mesenchymal cells that give rise to the pinna in humans.⁶ These observations suggest that, in the absence of Bcl2, excessive apoptosis in the fourth rhombomere of the neural crest or the second pharyngeal arch leads to a small pinna and malformed stapes. This theory fits with Nakayama's observation that *Bcl2* may be important in morphogenesis because it is expressed in condensations of cells committed to the formation of more complex structures.³ Other components of the *Bcl2*^{-/-} pleiotropic phenotype may be due to dysregulation of common progenitors such as neural crest cells. Disorders arising in neural crest in humans (neurocristopathies), such as Hirschsprung's disease, Waardenburg syndrome and Axenfeld-Rieger syndrome, are characterised by their pleiotropy.¹³ However, the *Bcl2*^{-/-} snub-shaped snout is not due to deficiency of second pharyngeal arch cells as the frontal bone and premaxillary bone are derived instead from the frontonasal process.¹²

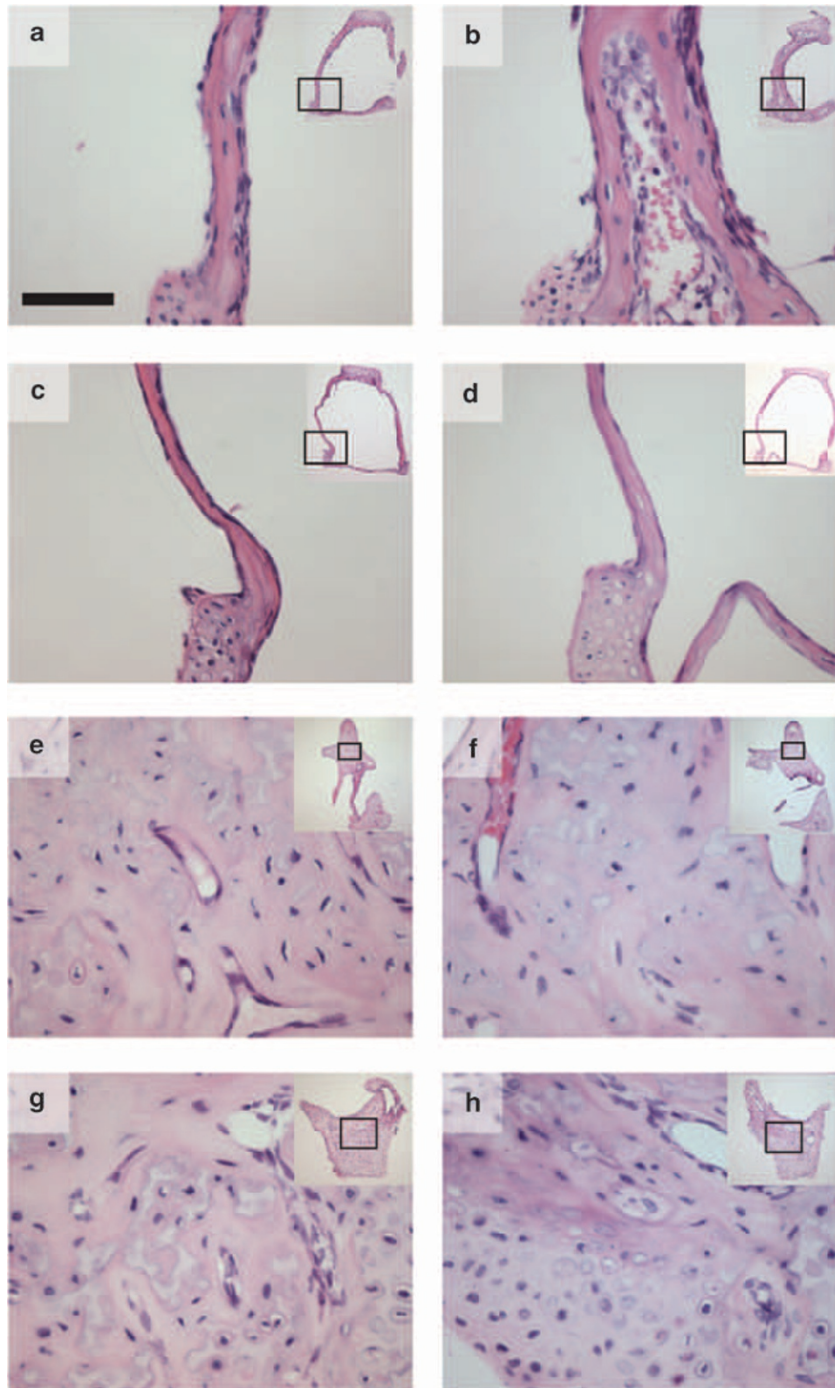


Figure 5 Light micrographs of ossicle sections stained with hematoxylin and eosin showing porosity of $Bcl2^{-/-}$ stapes but not malleus or incus. $Bcl2^{-/-} Bim^{+/-}$ and $Bcl2^{-/-} Bim^{-/-}$ stapes were not porous; (a) $Bcl2^{+/+} Bim^{+/+}$ stapes; (b) $Bcl2^{-/-} Bim^{+/+}$ stapes; (c) $Bcl2^{-/-} Bim^{-/-}$ stapes; (d) $Bcl2^{-/-} Bim^{+/-}$ stapes; (e) $Bcl2^{+/+} Bim^{+/+}$ malleus; (f) $Bcl2^{-/-} Bim^{+/+}$ malleus; (g) $Bcl2^{+/+} Bim^{+/+}$ incus; (h) $Bcl2^{-/-} Bim^{+/+}$ incus; inset, low-power micrograph with location of high-power micrograph indicated by box; all mice were 3–8 weeks of age; bar $50 \mu\text{m}$

$Bcl2$ is required for osteoclastogenesis and $Bcl2^{-/-}$ mice have fewer osteoclasts than wild-type mice.^{14,15} Furthermore, $Bcl2^{-/-}$ osteoclasts are larger and more short-lived than wild-type osteoclasts *in vitro*.¹⁵ The dearth of osteoclasts in $Bcl2^{-/-}$ mice leads to osteopetrosis (increased bone density) because there is insufficient bone remodelling.¹⁶

Decreased osteoclastic bone resorption in $Rankl^{-/-}$ and $c-fos^{-/-}$ mice results in ossicles being abnormally thick and cartilaginous, and causes approximately 30 dB SPL of hearing loss.¹⁷ Increased osteoclastic bone resorption in $Opg^{-/-}$ mice causes osteoporosis, leading to thinning of ossicles and mild, progressive hearing loss.¹⁸

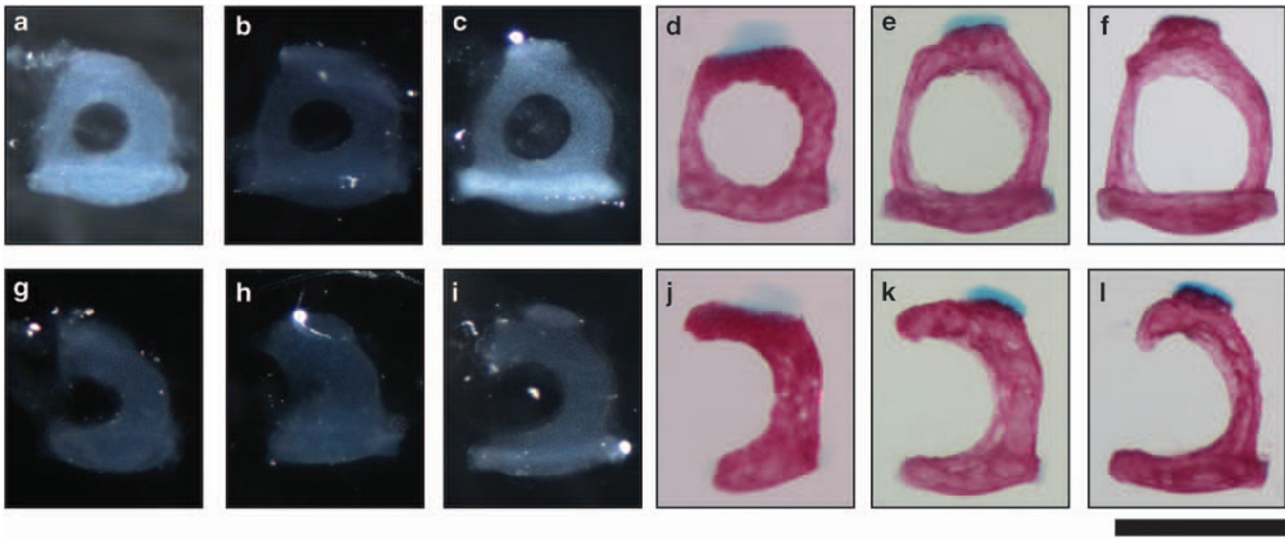


Figure 6 Stapes from skeletal preparations stained with alizarin red and alcian blue showing that *Bcl2*^{-/-} stapes is malformed at birth; upper panel, *Bcl2*^{+/+} and *Bcl2*^{+/-}; lower panel, *Bcl2*^{-/-}; (a and g) p0; (b and h) p1; (c and i) p4; (d and j) p7; (e and k) p13; (f and l) p21

Impaired osteoclastogenesis is unlikely to be the cause of the stapes defect in *Bcl2*^{-/-} mice for a number of reasons. Firstly, unlike in *Opg*^{-/-}, *Rankl*^{-/-} and *c-fos*^{-/-} mice, the malleus and incus are unaffected in *Bcl2*^{-/-} mice. Secondly, the *Bcl2*^{-/-} stapes are misshapened by p0, at which point the stapes is cartilaginous and bone remodelling has not commenced. Finally, the *Bcl2*^{-/-} stapes changes shape after ossification, indicating that some bone remodelling occurs in this ossicle.

The hearing loss observed in the *Bcl2*^{-/-} mouse is severe. Fusions of the stapes to the temporal bone, present in *Nog*^{+/-} mice, cause ~18 dB SPL of hearing loss,¹⁹ which is much milder than the >60 dB SPL hearing loss observed in *Bcl2*^{-/-} mice. Surgical fixation of mouse ossicles with cyanoacrylic cement produces ~20 dB SPL hearing loss at ~16 kHz,²⁰ while ossicular chain disruption behind an intact tympanic membrane can result in maximal hearing loss of 60 dB SPL.²¹ Thus, ossicular chain discontinuity is the likely cause of the severe *Bcl2*^{-/-} hearing loss. The *Bcl2*^{-/-} *Bim*^{+/-} stapes is only mildly misshapen and this mouse displays high-frequency hearing loss. Stapes movement is mainly piston-like at low frequencies but includes anterior–posterior rocking motions at high frequencies.²² The thickening of the anterior crus in the *Bcl2*^{-/-} *Bim*^{+/-} stapes likely affects the rocking but not the piston-like movements, resulting in high-frequency hearing loss.

Human congenital ossicle defects are rare, but when they do arise, the stapes is often the only bone affected.²³ Different human stapes abnormalities have been described but little is understood about their etiology. The severity and pleiotropy of the *Bcl2*^{-/-} mouse phenotype suggests that human stapes defects are unlikely to be caused by inherited, null alleles of *Bcl2*. However, our finding that Bcl2 is essential for stapes development implicates dysregulated apoptosis in human stapes abnormalities. In conclusion, Bcl2 is required for stapes development and the absence of Bcl2 leads to severe conductive hearing loss.

Materials and Methods

Mice. All mice were bred and maintained at the Walter and Eliza Hall Institute. The *Bcl2*^{-/-} strain³ and the *Bim*^{-/-} strain⁴ have been backcrossed more than 10 times to C57BL/6J. *Bcl2*^{+/-} *Bim*^{+/-} × *Bcl2*^{+/-} *Bim*^{+/-} and *Bcl2*^{-/-} *Bim*^{+/-} × *Bcl2*^{-/-} *Bim*^{-/-} matings generated experimental cohorts of mice. The Walter and Eliza Hall Institute animal ethics committee approved all experiments involving animals.

Genotyping. Genotyping of *Bcl2* was performed by polymerase chain reaction (PCR) with the primers 5'-CACGAGACTAGTGAGACGTGC-3', 5'-CTGAACCGG CATCTGCACACC-3' and 5'-CTAAAGATGCATAGGTC AAGAG-3'. Twenty μl reactions contained 10 pmol each primer, genomic DNA and 1 × GoTaq green master mix (Promega, Madison, WI, USA). Reactions were subjected to an initial denaturation of 94 °C for 4 min followed by 30 cycles of 94 °C for 40 s; 55 °C for 30 s; 72 °C for 1 min then final extension of 72 °C for 5 min. PCR product sizes were 405 bp for the wild-type allele and 700 bp for the knockout allele. Genotyping of *Bim* was performed as previously described.²⁴

Auditory brainstem response. Mice were anaesthetized by intraperitoneal injection of 100 mg/kg ketamine and 20 mg/kg xylazine and body temperature maintained at 37 °C with a heat pad in a sound-attenuated, electrically shielded room. A loud speaker was placed 10 cm from the pinna of the test ear, and computer-generated clicks and pure tone stimuli of 4, 8, 16 and 32 kHz (tone-pips, 1-ms rise/fall, 3-ms plateau) were presented with maximum intensities of 100–108 dB peak equivalent (p.e.) SPL. ABRs were recorded differentially using percutaneous stainless-steel needle electrodes positioned at the vertex of the skull (+ve) and on the snout (-ve) with a ground on the thorax. Signals were amplified by 10⁵ and band pass filtered (150 Hz–3 kHz). The output of the filter was fed to a 16-bit analogue-to-digital converter (series 2 model, Tucker Davis Technologies, Alachua, FL, USA) and sampled at 20 kHz for a period of 12.5 ms following the stimulus onset. ABRs were averaged over 500 repetitions of the clicks or tone-pips presented at 33/s. Stimulus intensity was incremented in 5 dB steps from sub-threshold levels. Average ABR traces were subsequently analyzed to determine ABR threshold using custom-written analysis routines (Dr. James Fallon) on commercial software (Igor Pro v6.04, WaveMetrics, Portland, OR, USA). The threshold was defined as the lowest intensity stimulus that reproducibly elicited a Wave III ABR (2.5–3 ms latency) using a visual detection criterion.²⁵

For electrically-evoked ABR the bulla was surgically exposed and a stimulating electrode placed on the round window and a returning electrode positioned within the bulla cavity. Optically-isolated, biphasic current pulses were delivered and the evoked activity was recorded as described above. The intensity of the electrical stimulus that produced a peak-trough response amplitude of at least 0.2 μV for the eABR was defined as threshold.

Histology. Mice were euthanized with CO₂. Phosphate-buffered saline (PBS) followed by 10% neutral-buffered formalin was perfused through each animal via a cannula inserted into the left ventricle. Cochleae and stapes were dissected from the temporal bones and post-fixed for 1 h at room temperature. Cochleae were then decalcified in 10% EDTA for 5 days at 4 °C. Cochleae and stapes were oriented in 1% agarose in PBS and embedded in paraffin. Sections (2 μm) were cut using a microtome and stained with hematoxylin and eosin. Sections were imaged on a light microscope (Axioplan II, Carl Zeiss, North Ryde, NSW, Australia). Spiral ganglion neuron density was determined by counting the number of neurons with prominent nucleoli in the Rosenthal's canal of the middle cochlear turn using Metamorph software (Molecular Devices Inc., Sunnyvale, CA, USA).

X-ray micro-computed tomography. X_μCT was conducted using the Xradia machine MicroXCT-200 (Xradia Inc., Pleasanton, CA, USA), located in the Department of Physics, La Trobe University. An X-ray closed tube source with a Tungsten target was operated at 60 kV tube voltage and power of 8W. The sample was placed at 100 mm from the source and 25 mm from the detector. The imaging detector was a charge-coupled device camera coupled with a scintillator system and × 10 objective lens. The sample was scanned by acquiring 361 projections at equal angles through an angular range of 180° using TXMController software (Xradia Inc.). Each projection image was recorded in 9 s. Each image was corrected for the dark current image and for the nonuniform illumination in the imaging system, determined by taking a reference image of the beam without sample. A filtered back projection algorithm was then used to reconstruct the acquisition data to create a three-dimensional image using TXMReconstructor software (Xradia Inc.). After the reconstruction process, the distribution of the linear attenuation coefficient was obtained along the section of the sample crossed by the radiation. The total reconstructed volume contained 512 × 512 × 512 voxels with the voxel size of (4.3 μm)³. Three-dimensional (3D) data was computed with TXM3Dviewer software (Xradia Inc.) and segmented with Avizo-6.2 software (Mercury Computer Systems Inc., Merignac Cedex, France).

Skeletal preparations. Mouse heads were placed in 80% ethanol for 4 days then in acetone for 4 days. After rinsing in water and 95% ethanol, heads were stained with 0.015% (w/v) alcian blue, 0.005% (w/v) alizarin red, 5% (v/v) acetic acid, 95% (v/v) ethanol for 10 days. Heads were cleared in 1% KOH for 16 h at 37 °C then at room temperature for 28 days. Stapes were dissected and photographed under a dissecting microscope.

Statistics. Student's two-tailed *t*-tests were performed using Microsoft Excel 2008 for Mac v 12.2.0 software (Redmond, WA, USA).

Conflict of Interest

The authors declare no conflict of interest.

Acknowledgements. We acknowledge the financial support of the Hearing CRC, established and supported under the Australian Government's Cooperative Research Centres Program, the Victorian State Government's Operational Infrastructure Support Program and the Australian Government's NHMRC IRIISS. MRC was supported by the Garnet Passe and Rodney Williams Memorial Foundation. AKW was supported by the National Institutes of Health (HHS-N-263-2007-00053-C). BDA acknowledges the support of the Australian Research Council through the Centre of Excellence for Coherent X-ray science. We thank Mathew Salzone, Priscilla Kennedy, and Emily Sutherland for technical assistance.

Author Contributions

MRC and RAB designed and performed experiments, analysed data and wrote the paper. AKW provided technical expertise and conducted electrophysiology experiments (ABR and eABR). BDA performed the X_μCT and segmentation analysis. PB provided the knockout mice and consulted on the study design. SM provided histological expertise and consulted on study design. MGM and AC

conducted experiments. All authors discussed the results and implications and commented on the manuscript.

1. Penaloza C, Orlanski S, Ye Y, Entezari-Zaher T, Javdan M, Zakeri Z. Cell death in mammalian development. *Curr Pharm Des* 2008; **14**: 184–196.
2. Youle RJ, Strasser A. The BCL-2 protein family: opposing activities that mediate cell death. *Nat Rev Mol Cell Biol* 2008; **9**: 47–59.
3. Nakayama K, Negishi I, Kuida K, Sawa H, Loh DY. Targeted disruption of Bcl-2 alpha beta in mice: occurrence of gray hair, polycystic kidney disease, and lymphocytopenia. *Proc Natl Acad Sci USA* 1994; **91**: 3700–3704.
4. Bouillet P, Metcalf D, Huang DC, Tarlinton DM, Kay TW, Kontgen F *et al*. Proapoptotic Bcl-2 relative Bim required for certain apoptotic responses, leukocyte homeostasis, and to preclude autoimmunity. *Science* 1999; **286**: 1735–1738.
5. Bouillet P, Cory S, Zhang LC, Strasser A, Adams JM. Degenerative disorders caused by Bcl-2 deficiency prevented by loss of its BH3-only antagonist Bim. *Dev Cell* 2001; **1**: 645–653.
6. LeBrun DP, Warnke RA, Cleary ML. Expression of bcl-2 in fetal tissues suggests a role in morphogenesis. *Am J Pathol* 1993; **142**: 743–753.
7. Brown SD, Hardisty-Hughes RE, Mburu P. Quiet as a mouse: dissecting the genetic and genetic basis of hearing. *Nat Rev Genet* 2008; **9**: 277–290.
8. Hockenbery DM, Zutter M, Hickey W, Nahm M, Korsmeyer SJ. BCL2 protein is topographically restricted in tissues characterized by apoptotic cell death. *Proc Natl Acad Sci U S A* 1991; **88**: 6961–6965.
9. Fallon JB, Irvine DR, Shepherd RK. Cochlear implant use following neonatal deafness influences the cochleotopic organization of the primary auditory cortex in cats. *J Comp Neurol* 2009; **512**: 101–114.
10. Mallo M. Formation of the outer and middle ear, molecular mechanisms. *Curr Top Dev Biol* 2003; **57**: 85–113.
11. Masuda Y, Honjo H, Naito M, Ogura Y. Normal development of the middle ear in the mouse: a light microscopic study of serial sections. *Acta Med Okayama* 1986; **40**: 201–207.
12. Santagati F, Rijli FM. Cranial neural crest and the building of the vertebrate head. *Nat Rev Neurosci* 2003; **4**: 806–818.
13. Bolane RP. The neurocristopathies: a unifying concept of disease arising in neural crest maldevelopment. *Hum Path* 1974; **5**: 409–429.
14. Nagase Y, Iwasawa M, Akiyama T, Kadono Y, Nakamura M, Oshima Y *et al*. Anti-apoptotic molecule Bcl-2 regulates the differentiation, activation, and survival of both osteoblasts and osteoclasts. *J Biol Chem* 2009; **284**: 36659–36669.
15. Yamashita J, Datta NS, Chun YH, Yang DY, Carey AA, Kreider JM *et al*. Role of Bcl2 in osteoclastogenesis and PTH anabolic actions in bone. *J Bone Miner Res* 2008; **23**: 621–632.
16. McGill GG, Horstmann M, Widlund HR, Du J, Motyckova G, Nishimura EK *et al*. Bcl2 regulation by the melanocyte master regulator Mitf modulates lineage survival and melanoma cell viability. *Cell* 2002; **109**: 707–718.
17. Kanzaki S, Takada Y, Niida S, Takeda Y, Udagawa N, Ogawa K *et al*. Impaired vibration of auditory ossicles in osteopetrotic mice. *Am J Pathol* 2011; **178**: 1270–1278.
18. Kanzaki S, Ito M, Takada Y, Ogawa K, Matsuo K. Resorption of auditory ossicles and hearing loss in mice lacking osteoprotegerin. *Bone* 2006; **39**: 414–419.
19. Hwang CH, Wu DK. Noggin heterozygous mice: an animal model for congenital conductive hearing loss in humans. *Hum Mol Genet* 2008; **17**: 844–853.
20. Qin Z, Wood M, Rosowski JJ. Measurement of conductive hearing loss in mice. *Hear Res* 2010; **263**: 93–103.
21. Austin DF. Ossicular reconstruction. *Otolaryngol Clin North Am* 1972; **5**: 145–160.
22. Heiland KE, Goode RL, Asai M, Huber AM. A human temporal bone study of stapes footplate movement. *Am J Otol* 1999; **20**: 81–86.
23. Park K, Choung YH. Isolated congenital ossicular anomalies. *Acta Otolaryngol* 2009; **129**: 419–422.
24. Egle A, Harris AW, Bouillet P, Cory S. Bim is a suppressor of Myc-induced mouse B cell leukemia. *Proc Natl Acad Sci USA* 2004; **101**: 6164–6169.
25. Coco A, Epp SB, Fallon JB, Xu J, Millard RE, Shepherd RK. Does cochlear implantation and electrical stimulation affect residual hair cells and spiral ganglion neurons? *Hear Res* 2007; **225**: 60–70.



Cell Death and Disease is an open-access journal published by Nature Publishing Group. This work is licensed under the Creative Commons Attribution-NonCommercial-No Derivative Works 3.0 Unported License. To view a copy of this license, visit <http://creativecommons.org/licenses/by-nc-nd/3.0/>

Supplementary Information accompanies the paper on Cell Death and Disease website (<http://www.nature.com/cddis>)